Thesis for the Degree of Licentiate of Engineering

Large eddy simulation using linear eddy sub-grid mixing modeling

Salman Arshad

Department of Combustion
Chalmers University of Technology
Göteborg, Sweden 2016

Large eddy simulation using linear eddy sub-grid mixing modeling
Salman Arshad

Technical report number: 08/2016
ISSN 1652-8565

Department of Combustion
Chalmers University of Technology
SE–412 96 Göteborg
Sweden
Telephone: +46 (0)31 – 772 1000

Typeset by the author using LaTeX.

Chalmers Reproservice
Göteborg, Sweden 2016

Abstract

As emissions regulations are getting stricter and efficiency requirements of engines are increasing, different concepts to improve combustion are being investigated. For example lean stratified premixed combustion, homogeneous charge compression ignition(HCCI), use of more exhaust gas recirculation (EGR) to reduce NOx etc. In all these concepts, combustion happens at lower temperatures, higher pressures, and higher level of air dilution than today's typical spark ignition or diesel engines.

Many combustion models in computational fluid dynamics (CFD) today describe either premixed or non-premixed mode of combustion, assuming fast chemistry regimes only. There is a great need of new combustion models that are mode (premixed/non-premixed) and regime (fast/non fast chemistry) independent. The linear eddy model (LEM) of Kerstein [1] used as a sub-grid combustion model for large eddy simulation (LES) is regarded as a truly mode and regime independent combustion model as it models all the physical processes, i.e. large and small scale turbulent advection, molecular diffusion and chemical reactions at their respective time scales. It is also crucial for combustion models to describe turbulent mixing well. The LEM used as a sub-grid mixing model for LES called LES-LEM, has been successfully used to predict turbulent mixing flows too.

This thesis presents a new approach for large scale turbulent advection in LES-LEM. The approach links the sub-grid LEM implementation to a concept of control-volume crossing rate. Magnitude and direction of the crossing is implied by LES-prescribed mass fluxes. A high flux implies a high crossing rate, corresponding to a high displacement per time step, and vice versa.

List of publications

This thesis is based on the following appended paper:

Paper 1

Salman Arshad, Bo Kong, Alan Kerstein, Michael Oevermann, "A strategy for large-scale scalar advection in large eddy simulations that use the linear eddy sub-grid model", *ICCHMT 2016*, May 2016, Cracow, Poland.

Acknowledgments

First of all, I would like to express my special thanks to my supervisor Professor Michael Oevermann for his guidance, great support, all the fruitful discussions and patience. My warm thanks goes to Alan Kerstein for all the great ideas and explanations.

Thanks to Professor Ingemar Denbratt for giving me the chance to work on this interesting PhD project at the division of combustion.

I would like to thank the Swedish Research Council for financial support of the project. In addition, thanks to the Swedish National Infrastructure for Computing (SNIC) at C3SE Chalmers for providing resources for the simulations.

Many thanks to Tim Lackmann for support, interesting discussions and good time. I am really happy to share my office with him.

Thanks to all my colleagues in the combustion division, especially to Boxiong Chen. Moreover I would like to thank my Pakistani friends in Sweden for fun times.

Finally, I would thank from the bottom of my heart to my whole family. Thanks for all the support throughout my life.

Contents

Chapter 1

Introduction

1.1 Motivation

Combustion has been used by humans for thousands of years for practical purposes of cooking food and heating homes. With advent of the steam engine, a new use of combustion was found, i.e. to produce work. Steam engines were used particularly in railroads and steam ships. After the discovery of gasoline, steam engines were replaced with internal combustion engines (ICE), which are still being used extensively for e.g. transportation and power generation purposes. However, tremendous use of ICE has lead to various environmental and health hazards. So modern research on combustion in ICE has two major objectives, i.e. the optimization of combustion efficiency and the reduction of pollutants. In order to achieve these objectives, a clear understanding of the processes taking place during combustion is a prerequisite. This understanding will only be obtained by a joint approach of experiments and modeling.

As emissions regulations are getting stricter, different concepts to improve combustion and reducing tailpipe emissions in ICE are being studied. For example, to reduce NOx in spark-ignition engines, lean air-fuel mixture is used and to reduce NOx in diesel engines, more exhaust gas recirculation (EGR) is being used. Other concepts of improving combustion by having a low temperature combustion process are also being investigated. Many current combustion models in computational fluid dynamics (CFD) assume fast chemistry regimes and are aimed to describe either premixed or non-premixed modes of combustion. However, future engines will most likely operate at lower temperatures, higher pressures, and higher level of air dilution than today's engines. So most combustion models used today might not adequately predict combustion under those operating conditions that take place in unconventional mixed-mode and turbulent combustion regimes. The basic requirement for a mode and regime independent turbu-

lent combustion model is that it should accurately represent the interactions between small and large scale turbulence, chemistry and molecular diffusion.

1.1.1 Large eddy simulation (LES)

Large eddy simulation (LES) is a popular CFD method that resolves the energy containing large-scale turbulent motion directly and models the effect of unresolved small scales, resulting in lower grid resolution requirements than for direct numerical simulation (DNS). For scalar mixing, LES has shown better predictive capabilities than Reynolds Averaged Navier Stokes (RANS) approaches [3]. LES has shown a good predictive capability in many studies related to ICE. Just a few examples include work done by Jhavar and Rutland [4] about the investigation of cycle-to-cycle variations in HCCI engines using the well stirred reactor model. Adomeit et. al [5] studied the influence of cycle-to-cycle variations of inlet conditions on the fuel-air mixing process in a direct injection spark ignition (DISI) engine. LES simulations employing the progress variable approach (to model turbulent combustion) were used to study turbulent flows in diesel engines [6] and lean ethanol/air mixtures in HCCI engines [7, 8]. Other examples of LES studies of ICE can be found in the review paper of Rutland [9].

1.1.2 LES-LEM

One combustion model which has been successfully applied to both premixed and non-premixed combustion and can be regarded as a truly mode (premixed/non-premixed) and regime (fast/non fast chemistry) independent is the linear eddy model (LEM) of Kerstein [1] used as a sub-grid combustion model for LES. Kerstein [1] formulated the Linear Eddy Model (LEM) as a scalar mixing model for non-reacting flows and then extended it to predict reactive flows [10]. LEM resolves all spatial and temporal scales on a one-dimensional line and simulates turbulent advection, molecular diffusion, and chemical reaction on that line. LEM has been used both as a stand-alone tool and as an LES sub-grid model (LES-LEM).

In LES-LEM, physical processes, i.e. large and small scale turbulent advection, molecular diffusion and chemical reaction are modeled at their respective time scales. LES-LEM has been demonstrated to successfully simulate turbulent scalar mixing by McMurtry et al. [15], non-premixed turbulent combustion by Calhoon [16] and Menon and Calhoon [17], and premixed turbulent combustion by Smith [18] and Chakravarthy and Menon [19]. LES-LEM was extended by including two fluid models for spray combustion by Pannala and Menon [20] and by including radiative heat loss and soot modeling by Zimberg et al. [21]. Sankaran and Menon [22] predicted a

premixed turbulent methane/air flame using LES-LEM. Sen and Menon employed LES-LEM to simulate different premixed and non-premixed flames by using an artificial neural network approach for speeding up the chemistry [23,24]. The SANDIA non-premixed piloted methane/air flame D was simulated with LES-LEM using a low-Mach number formulation for LES by Ochoa et al. [25].

Work done related to reciprocating engines include the LES-LEM implementation in KIVA for simulating a direct injection spark ignition engine [26] and an URANS-LEM approach to investigate pressure histories in an automotive HCCI engine [27]. Maxwell [28] used compressible LES-LEM to assess gaseous explosion hazards. Turbulent combustion of hydrogen-enriched fuels was studied by Martinez et al. [29] [30] using LES-LEM. Lovett et al. studied flame structure of bluff-body stabilized flames [31]. Srinivasan et al. [32] used LES-LEM for spray combustion simulations and to investigate combustion instabilities in a continuous variable resonance combustor [33]. Furthermore, LES-LEM is capable of predicting extinction and re-ignition effects [24] due to direct interaction of turbulent advection with diffusion and chemical reactions.

1.1.3 Passive scalar mixing

The cited literature above indicates that the main application of LES-LEM so far has been related to turbulent combustion which, of course, heavily depends on the capability of LES-LEM to predict scalar mixing reasonably well.

Several studies have been done on scalar mixing. A few examples of DNS studies of passive scalar mixing include work done by Vedula et al. [34] and Donzis and Yeung [35]. Cha et al. [36] performed DNS of passive scalar mixing in a double scalar mixing layer and Sawford and Kops [37] studied DNS of ternary mixing. Many LES studies on scalar mixing, model the subgrid scalar flux using the standard gradient diffusion approximation, which employs the turbulent Schmidt number. Examples of these LES studies, using the standard eddy diffusivity modeling approach include work done by Akselvoll and Moin [38], Kang and Meneveau [39], Dong et al. [40], and Philips et al. [41]. In a recent study Mejia et al. [42] did LES simulations of passive scalar mixing in a high Schmidt number turbulent jet and compared the eddy diffusivity model having constant and dynamic turbulent Schmidt numbers to an anisotropy model.

1.2 Objectives

The standard LES sub-grid mixing models do not represent turbulent mixing in a proper way because they do not adequately represent molecular diffusion processes and counter gradient effects. Turbulent mixing consists of two different processes, i.e. turbulent stirring which increase the interface between unmixed species and molecular diffusion. It is crucial to model these two processes individually at their respective time scales. LEM explicitly include both of these processes and has been used successfully as a sub-grid scalar mixing model [15] [26].

However, in this thesis the turbulent mixing capabilities of LES-LEM with a modified splicing treatment are examined. It is important to note that this is the first LES-LEM implementation for an unstructured grid.

Therefore, the objective of this thesis is to demonstrate the predictive capabilities of LES-LEM with the new splicing approach for passive scalar mixing.

1.3 Thesis outline

The thesis has four chapters.

The first provides a brief introduction to LES-LEM and scalar mixing.

The second part describes the mathematics underpinning turbulent mixing, LES, LEM, LEM as a sub-grid scalar mixing model for LES, the new splicing approach in detail and coupling of LES-LEM.

The third part presents some results obtained for passive scalar mixing using LES-LEM with the modified splicing.

The fourth part presents LES equations for combustion (variable density and non-isothermal flow) and coupling to LEM sub-grid combustion model.

Chapter 2

Mathematical model

This chapter introduces the governing equations used to describe turbulent mixing flows, LES and then presents the linear eddy model (LEM). The details of LES-LEM implementation are discussed at the later sections of this chapter.

2.1 Turbulent mixing

Most of the fluid flows that we encounter daily are turbulent in nature. In turbulent flows, momentum forces are larger than viscous forces thus causing irregular and chaotic motion. There exists a large range of scales in the turbulent flow, ranging from the large structures of the flow to the smallest energy dissipating eddies. The governing equations of turbulent flow are the Navier-Stokes and the continuity equations. For incompressible flow, these equations are:

$$\frac{\partial u_i}{\partial t} + u_j \frac{\partial u_i}{\partial x_j} = -\frac{1}{\rho}\frac{\partial p}{\partial x_i} + \nu \frac{\partial^2 u_i}{\partial x_j x_j},$$
$$\frac{\partial u_i}{\partial x_i} = 0,$$

where t, p, ρ, ν and u_i denote time, pressure, density, viscosity and velocity components respectively, and x_i are spatial coordinates. An important property of turbulence is its ability to mix passive scalars at higher rates than in laminar flow. A passive scalar is a contaminant that has absolutely no influence on the flow but is transported by the flow. Passive scalar mixing in turbulent flow is an important phenomenon and is encountered in many flow problems, e.g. heat transfer, pollutant dispersion in the environment, combustion, and production processes in chemical reaction engineering. Fundamental understanding of basic processes involved in turbulent

scalar mixing is crucial for predicting mixing processes which is beneficial for many applications.

2.2 Large Eddy Simulation (LES)

Computational Fluid Dynamics (CFD) models can be useful tools for studying mixing problems but they need to be validated against experimental data. In CFD, the governing equations are numerically solved. The computational domain is divided into a finite number of parts on which the governing equations are discretized and then solved. In direct numerical simulation (DNS), the domain is resolved to the smallest scales of the flow and is thus computationally non-feasible for practical flow problems. Large eddy simulation (LES) is a popular CFD method for turbulent flow simulation. LES resolves the energy containing large-scale turbulent motion directly and models the effect of unresolved small scales, resulting in lower grid resolution requirements than for DNS. For scalar mixing, LES has shown better predictive capabilities than Reynolds Averaged Navier Stokes (RANS) approaches [3]. In LES, large scales of the flow are separated from the smaller scales of the flow by applying a spatial filter on the governing equations. Filtering the Navier-Stokes and the continuity equations result in a set of governing equations for the resolved scales and is given as:

$$\frac{\partial \overline{u}_i}{\partial t} + \frac{\partial (\overline{u}_i \overline{u}_j)}{\partial x_j} = -\frac{1}{\rho}\frac{\partial \overline{p}}{\partial x_i} + \nu \frac{\partial}{x_j}\left(\frac{\partial \overline{u}_i}{\partial x_j} + \frac{\partial \overline{u}_j}{\partial x_i}\right) - \frac{\partial \tau_{ij}}{\partial x_j},$$
$$\frac{\partial \overline{u}_i}{\partial x_i} = 0,$$

where $(\overline{*})$ means filtered values and τ_{ij} is the turbulent sub-grid stress tensor defined as:

$$\tau_{ij} = \overline{u_i u_j} - \overline{u}_i \overline{u}_j,$$

τ_{ij} includes sub-grid scale information and a sub-grid model is required for it.

2.2.1 Sub-grid modeling

The simplest sub-gird scale models are based on hypothesis that the effect of unresolved scales is an enhanced viscosity and are known as eddy-viscosity models given by:

$$\tau_{ij} - \frac{1}{3}\tau_{kk}\delta_{ij} = -\nu_{sgs}\left(\frac{\partial \overline{u}_i}{\partial x_j} + \frac{\partial \overline{u}_j}{\partial x_i}\right) = -2\nu_{sgs}\overline{S}_{ij},$$

where ν_{sgs} is the eddy viscosity and $\overline{S}_{ij}$ is the resolved rate of strain tensor.

A popular eddy viscosity model is the Smagorinsky model proposed by Smagorinsky [43]. In this model, a relation for the eddy viscosity is obtained by assuming equilibrium between sub-grid scale energy production and dissipation. The relation is given by:

$$\nu_{sgs} = (C_s\overline{\Delta})^2 \mid \overline{S} \mid,$$

where

$$\mid \overline{S} \mid = \sqrt{2\overline{S}_{ij}\overline{S}_{ij}},$$

and $\overline{\Delta}$ is the effective filter width defined as:

$$\overline{\Delta} = (\Delta_1\Delta_2\Delta_3)^{1/3},$$

Δ_1, Δ_2 and Δ_3 are the filter widths in x, y and z direction respectively. $\overline{S}_{ij}$ is the filtered rate of deformation tensor defined as:

$$\overline{S}_{ij} = \frac{1}{2}\left(\frac{\partial\overline{u}_i}{\partial x_j} + \frac{\partial\overline{u}_j}{\partial x_i}\right),$$

The value of the constant C_s is generally between 0.1 and 0.2.

The one-equation model is another eddy viscosity model proposed by Yoshizawa [44] in which a balance equation for the sub-grid kinetic energy is solved:

$$\frac{\partial k_{sgs}}{\partial t} + \overline{u}_j\frac{\partial k_{sgs}}{\partial x_j} = \nu_{sgs} \mid \overline{S} \mid^2 - \epsilon + \frac{\partial}{\partial x_j}\left(\nu_{eff}\frac{\partial k_{sgs}}{\partial x_j}\right),$$

where the effective viscosity ν_{eff} is sum of the eddy viscosity ν_{sgs} and the molecular viscosity. The eddy viscosity ν_{sgs} is given by:

$$\nu_{sgs} = C_k\overline{\Delta}\sqrt{k_{sgs}},$$

and the dissipation rate ϵ is given by:

$$\epsilon = C_\epsilon\frac{k_{sgs}^{3/2}}{\overline{\Delta}},$$

Here, C_k and C_ϵ are the two model constants.

The dynamic Smagorinsky model was proposed by Germano [45] and then improved by Lilly [46]. In this model, the model constant C_s is calculated as a function of space and time. The model applies a second filter, where the second filter width $\tilde{\Delta}$ is greater than the grid filter width $\overline{\Delta}$. The model assumes that sub-grid tensors from both the filtering operations can be modelled similarly. The dynamic model allows the eddy viscosity to reach zero near solid walls and in regions of laminar flow. The dynamic method can also be applied to other sub-grid viscosity models e.g. to dynamically calculate the constants C_k and C_ϵ in the one-equation eddy model.

2.3 The Linear Eddy Model

Kerstein [1] developed the Linear Eddy Model (LEM) with the motivation that, in order to accurately represent turbulent combustion, a model should be able to represent all relevant physical processes, notably turbulent advection, molecular diffusion, and chemical reaction. LEM resolves and simulates on a one-dimensional line all these processes at their relevant length and time scales hence reducing the computational cost relative to three-dimensional DNS while retaining high resolution. The effects of realistic 3D turbulence on the scalar field are modeled via instantaneous mapping events using 3D scaling laws. Several studies by Kerstein [10]- [14] have shown LEM to be a reliable, economical mixing model. In these studies an incompressible LEM formulation was used.

2.4 LES-LEM

In incompressible LES-LEM, the filtered Navier Stokes equations are numerically solved in Eulerian form on a 3D LES grid. Conservation equations for passive scalars are not solved on the resolved LES grid but instead are solved on the sub-grid LEM line. Turbulent passive scalar advection is divided into two parts, i.e. large scale advection with the resolved velocity field and sub-grid small scale turbulent advection. The scales for large scale advection range from the size of the integral scale down to the resolved LES scales while the small scales range from the grid resolution scale down to the Kolmogorov scale within the LEM domain residing in each LES cell. Large scale passive scalar advection is modeled by Lagrangian mass transport across LES cell faces while conserving mass and energy. LEM simulates the sub-grid scale turbulent advection and solves numerically the passive scalar diffusion equation on the one-dimensional line.

2.4.1 Molecular Diffusion

In LEM a diffusion equation for the passive scalar Y is solved on the one-dimensional line as:

$$\frac{\partial Y}{\partial t} = D\frac{\partial^2 Y}{\partial x^2},$$

2.4.2 Sub-grid scale turbulent advection

Sub-grid scale turbulent advection is modeled by stochastic re-arrangement events called triplet maps. Triplet maps model the effect of the sub-grid

velocity field on the sub-grid scalar field and represent the action of turbulent eddies on the sub-grid scalar field. Figure 2.1 taken originally from [47] shows the modelling of eddies using triplet maps. The top of Figure 2.1 shows a plane material surface having separate species A and B. The horizontal lines represent the initial concentration isopleths. Also initially, the concentration profile is uniform gradient shown by the straight line in the dashed box. The bottom part of Figure 2.1 shows the action of an eddy on the concentration isopleths.

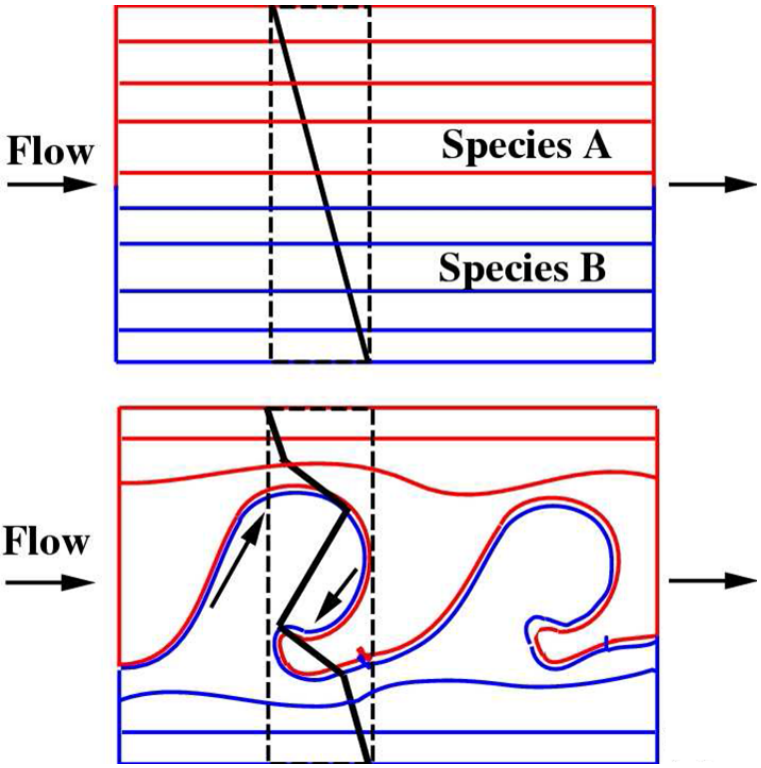

Figure 2.1: Schematics of the effect of an eddy [47]

The scalar field after triplet mapping is continuous and the map is measure preserving, which means that triplet maps do not create or destroy mass or energy but just re-arrange the scalar data on the one-dimensional LEM line. The mapping procedure first makes three copies of the selected segment (which represents the region affected by an eddy) and then each copy is compressed by a factor of 3. Lastly the middle copy is flipped to ensure a continuous profile.

Triplet mapping needs three parameters: i) eddy size l, ii) location of the eddy on the LEM line and iii) a mapping event rate per unit length. The location of an eddy is chosen randomly from a uniform distribution. Assuming inertial range scaling, the eddy size is sampled from an eddy size

distribution given by:

$$f(l) = \frac{5}{3}\frac{l^{-\frac{8}{3}}}{(\eta^{-\frac{5}{3}} - \Delta^{-\frac{5}{3}})},$$

Eddy sizes range from the local LES filter width Δ down to the Kolmogorov scale η. Here η is determined from the local sub-grid scale Reynolds number Re_Δ assuming inertial range scaling:

$$\eta = N_\eta \frac{\Delta}{(Re_\Delta)^{\frac{3}{4}}},$$

where N_η is an empirical constant and Re_Δ is given by:

$$Re_\Delta = \frac{u'\Delta}{\nu},$$

Here, ν denotes the kinematic viscosity and u' is a characteristic velocity fluctuation determined from the local sub-grid turbulent kinetic energy which is updated in the LES during every time step.

The eddy event rate per unit length is given by:

$$\lambda = \frac{54}{5}\frac{\nu Re_\Delta}{C_\lambda \Delta^3}\frac{\left[\left(\frac{\Delta}{\eta}\right)^{\frac{5}{3}} - 1\right]}{\left[1 - \left(\frac{\eta}{\Delta}\right)^{\frac{4}{3}}\right]}, \tag{2.1}$$

with the constants $C_\lambda = 15$ and $N_\eta = 3.0$. The average time interval between mapping (turbulent stirring) events is given by:

$$\Delta t_{stir} = \frac{1}{\lambda \Delta},$$

and the actual eddy time interval is sampled from a Poisson process.

2.4.3 Large scale advection

Large scale advection is represented by an approach called splicing. Splicing satisfies conservation of mass and transports mass across LES cell faces in a Lagrangian way. Splicing accounts for mass fluxes across LES cell faces and is implemented via Lagrangian transport of LEM cells between LES control volumes. This method requires three quantities:

1. The magnitude of mass to be transported across each LES cell face.
2. The direction of mass transport on each LES cell face i.e. outflux or influx.

3. An algorithm for ordering of splicing operations.

Total mass to be transferred across each LES cell face has two contributions, a sub-grid mass due to the unresolved velocity fluctuation and a resolved mass due to the resolved velocity field. The sub-grid mass contribution is given by:

$$M_{sgs} = \frac{\Delta t_{LES} A_{LES} u_{sgs}}{V_{LES}} M_{LEM}, \tag{2.2}$$

where Δt_{LES} is the LES time step, A_{LES} is the LES face area and u_{sgs} denotes the sub-grid scale velocity determined from the sub-grid turbulent kinetic energy k_{sgs} per unit mass via $u_{sgs} = \sqrt{\frac{2}{3} k_{sgs}}$. V_{LES} and M_{LEM} denote the LES cell volume of splicing donor and the total mass of LEM line of splicing donor, respectively. The direction of the sub-grid mass contribution is chosen randomly.

The resolved mass contribution for total splicing mass is given in analogy to equation (2.2) by:

$$M_{res} = \frac{\Delta t_{LES} A_{LES} u_{LES}}{V_{LES}} M_{LEM}, \tag{2.3}$$

where u_{LES} is the LES resolved velocity on the LES cell face. The direction of the resolved mass contribution is given by the direction of u_{LES}.

Figure 2.2 illustrates the splicing process.

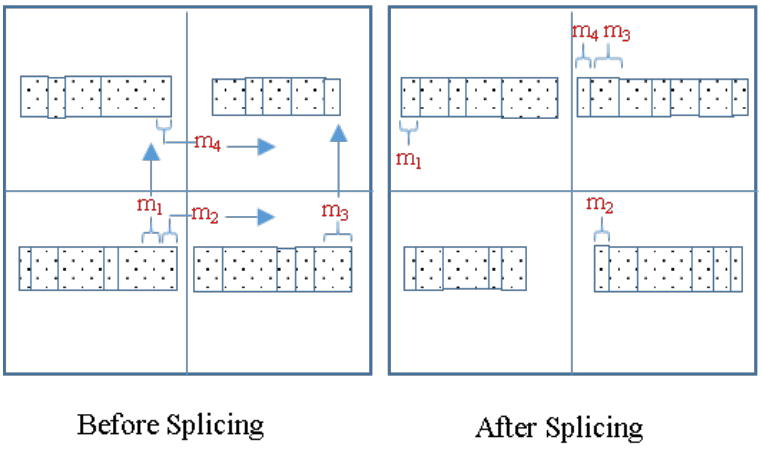

Figure 2.2: Schematics of the splicing process.

New splicing algorithm

The sum of equations (2.2) and (2.3) gives the mass to be transferred across an LES cell face during splicing. Also the direction of transfer is determined, so the face has an outflow and an inflow side. The LEM domain in the outflow cell provides the needed mass. This is done by removing a contiguous interval (segment) of the LEM domain on the outflow side of the LES cell face and attaching it to the LEM domain on the inflow side of the LES cell face.

Because each LES cell has many faces, there will typically be multiple outflows and inflows associated with a given LES cell. Some rationale is needed to determine the locations and sequencing of the removals and attachments of the segments crossing the various faces of a given LES cell.

This depends first on the chosen structure of the LEM domain. Topologically, the choices are a loop, corresponding to periodic boundary conditions, or a line segment. Here, as in most of the cited previous work, a line segment is used, with input and output sites at the respective endpoints of the line segment. This is a desirable choice because it tends to enforce consistency of the residence time of LEM fluid elements, which extends from the time of attachment to the LEM domain to the time of eventual removal. This point is illustrated by considering the alternative choice of attaching and removing fluxed segments at the same endpoint. Then the residence-time distribution would be highly skewed, with a strong peak at short residence time and a long tail reflecting fluid retained for a long time near the other endpoint, which is effectively an unphysical stagnation point. This is not only counter-intuitive, but introduces model artifacts. In Eulerian schemes, the CFL constraint is associated with the requirement that fluid should not be algorithmically propagated through multiple control volumes during one time step. This is a numerical instability mechanism as well as unphysical. Attachment and removal at the same LEM endpoint could propagate some fluid through multiple control volumes during one time step because the total number of attachments and removals per LEM domain equals the number of LES cell faces, which is six in a Cartesian mesh and typically more in an unstructured mesh, allowing a possible 'bucket brigade' scenario. Avoidance of this would require time step reduction far below the permissible CFL time step for an Eulerian transport scheme.

The mean residence time is dictated by the LES-prescribed mass-flux time history, so the degree of freedom available to avoid this artifact is the residence-time distribution, which should be as narrow as possible to minimize residence-time fluctuations. Designating each LEM domain endpoint as solely an input or an output location assures that fluid must pass through the domain between its attachment and removal times, thus avoiding the

short-residence-time scenario.

A feature of this approach is that it links the sub-grid LEM implementation to the concept of control-volume crossing rate. This can be developed further by considering the directionality of the crossing rate that is implied by the direction dependence of the LES-prescribed mass fluxes. High flux implies high crossing rate, corresponding to high displacement per time step, and vice versa. High flux also implies the transfer of a relatively large mass of the LEM domain across an LES cell face. It follows that larger mass transfers undergo more displacement, and vice versa, as illustrated in Figure 2.3.

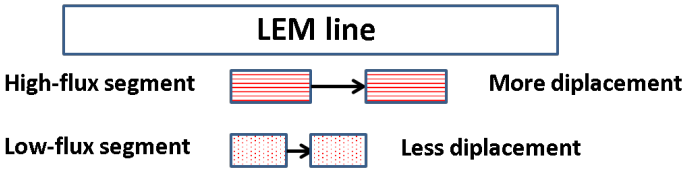

Figure 2.3: Principle of splicing algorithm

Figures 2.4 and 2.5 show how this principle is applied to the sequencing of segment removals and attachments during splicing. The segments to be spliced are considered as flowing along the LEM domain (meaning starting from the domain state prior to modification by splicing) and being ejected from the domain through the output boundary, and thus available for transfer across an LES face. For the lower-flux segments to flow a shorter distance than the higher-flux segments, they need to be closer to the output boundary and the high-flux segments need to be farther from that boundary. This implies that the ordering of removal is first the lowest-flux segments and then the higher-flux segments as shown in Figure 2.4.

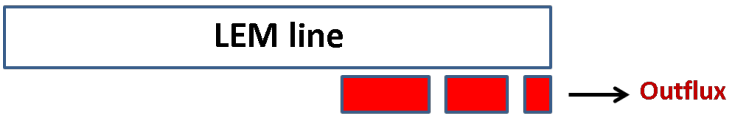

Figure 2.4: Order of removal of the LEM segments from the output boundary on the basis of flux

Using the same principle, the highest-flux segments are attached first to the inflow side of LEM line, followed by the lower-flux segments as shown in Figure 2.5.

Each LES cell has a sub-grid LEM domain. The new splicing algorithm is implemented by looping three times over all LES cells in the whole computational domain. During the first loop, the magnitude and direction of

Figure 2.5: Order of joining of the LEM segments to the input boundary on the basis of flux

mass flux on each LES cell face are calculated. An empty list is attached to each LES face. In the second loop, all outflux faces of an LES cell are identified and their respective outflux masses are gathered and sorted in ascending order. Then the outflux LEM segments corresponding to the outflux masses are spliced (cut and paste) in ascending order of outflux mass from the splicing donor LEM line to the corresponding empty lists (attached to each LES face). This procedure is repeated for all other LES cells until the second loop is finished and all the empty lists are now filled. Using the same principle, in the third loop, all the influx faces of a LES cell are recognized and their respective influx masses are sorted in descending order. Then the LEM segments are spliced in descending order (of influx mass) to the splicing receiver LEM line from the corresponding filled lists (attached to each LES face). The third loop goes through all LES cells and in the end all the filled lists resulting from the first loop are empty again. The splicing process is complete.

Parallel splicing

LES-LEM is computationally expensive and is not feasible without parallel computation. The standard splicing algorithm on a single processor domain has been implemented very efficiently using a pointer based LEM data structure where splicing is realized via simple pointer re-arrangements. However, domain decomposition for parallel computations on distributed memory architectures leads to processor domains which have a priori no input from neighboring processor domains. If splicing is not done correctly (e.g. by a simplified cell averaged approach) at processor boundaries, it can lead to unphysical results.

In order to perform splicing across processor boundaries, LEM lines across processor boundaries (called ghost LEM lines) are copied to the neighboring processor. Then splicing is performed between LEM lines that are next to the boundary and the ghost LEM lines by each processor.

Splicing at inlet and outlet boundaries

For LES cells at the inlet boundary, inlet mass needs to be added to their respective LEM lines. This inlet spliced mass is calculated using the same equations (2.2) and (2.3) and is added on the influx side of the LEM line. The remaining properties of this added fluid are taken from the inlet boundary. For inlet splicing mass calculations, the direction of the sub-grid mass contribution (equation (2.2)) is taken to be influx.

For the outlet boundaries, the calculated outlet splicing mass is removed from the outflux side of the LEM line. For outlet splicing mass calculations, the direction of the sub-grid mass contribution (equation (2.2)) is taken to be outflux.

The splicing algorithm explained above identifies different types of faces and it performs the corresponding type of splicing on that face, i.e. internal, processor boundary, inlet boundary and outlet boundary face.

2.4.4 LES-LEM coupling

In LES-LEM, the resolved LES field provides the sub-grid turbulent kinetic energy to each sub-grid LEM (for calculating the mapping event rate in equation (2.1)) and the LES time step (for advancing the LEM sub-grid simulations commensurately). The LEM provides a filtered passive scalar value to the LES cell. As no passive scalar equation is solved on the LES side, this is strictly output data representing the LES resolved passive scalar field.

One full time step of LES-LEM simulation consists of the following steps:

- In each LES cell, advance (till the LES time step) the sub-grid LEM , i.e. molecular diffusion and sub-grid turbulent advection via triplet maps.
- For each processor, get the updated (after sub-grid LEM simulations) ghost LEM lines from the neighboring processors.
- Predict the LES velocity field with the old time pressure field.
- Perform splicing based on the predicted LES velocity field.
- Correct the LES velocity field in a PISO pressure correction loop.
- Update the turbulence parameters.
- Perform splicing with the correct LES velocity field and updated sub-grid turbulent kinetic energy field.

- Re-grid the LEM. As splicing can result in transport of fractional LEM cells, the number of LEM cells in a LES cell are different than they were before the splicing operation. The numerical scheme used for the sub-grid molecular diffusion equation assumes a uniform grid so the LEM line in each LES cell is re-gridded to a uniform cell size having the same number (initial number) of LEM cells.

Chapter 3

Model validation

This chapter presents the results obtained for a passive scalar mixing test case using LES-LEM with the new splicing approach.

3.1 Numerical set-up

The modified splicing approach was tested by doing simulations of passive scalar transport in a co-flowing confined rectangular liquid jet in OpenFOAM 2.0.x. Figure 3.1 taken originally from [2] shows the test section of the jet. Kong et al. [2] performed LES simulations of the same case earlier and compared the LES results with the particle image velocimetry (PIV) measurements. The Reynolds number is 20,000 and the inlet streams have velocities of 0.2, 0.4 and 0.2 m/s respectively. The passive scalar Rhodamine 6G was injected only in the middle stream while the outer two streams were pure water.

This thesis extends the work of Kong et al. [2] by adding passive scalar transport while the numerical setup for the LES remains the same (i.e. computational domain, grid size, inlet conditioning technique, interpolation schemes, gradient schemes and boundary conditions). The computational domain has dimensions of 0.3 x 0.06 x 0.1 m^3 having 240 x 90 x 110 cells in x, y and z direction, respectively. The linear interpolation schemes and a second order least squares gradient scheme are used. The fixed walls are treated as no-slip and wall functions are used for the boundary layers. The exit uses a convective outflow boundary condition. Zero gauge pressure is specified at the outlet. Zero gradient condition is used for pressure at the walls and the inflow boundary.

The approximate Kolmogorov scale reported for the experiments was 94.5 μm [48]. The Schmidt (Sc) number, defined as the ratio of momentum diffusivity (viscosity) and mass diffusivity, has the value of $\sim$2420 based on

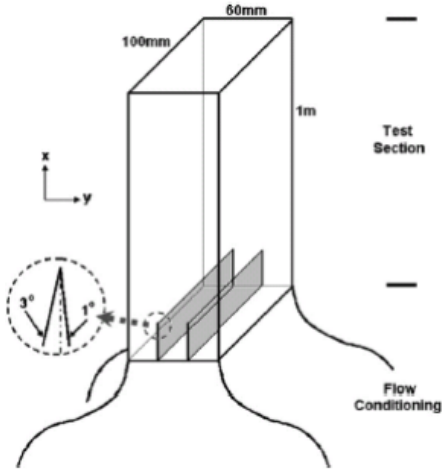

Figure 3.1: Schematics of jet test section [2]

values of the kinematic viscosity of water at 25 degree Celsius of 1x10^{-6} (m^2/s) and the diffusion coefficient of passive scalar Rhodamine 6G in water of 4.14x10^{-10} (m^2/s). In order for the LEM to fully resolve the Kolmogorov scale, approximately 60 LEM cells were required. The Batchelor scale (scalar resolution scale) is smaller than the Kolmogorov scale by the factor $Sc^{-0.5}$, so even resolving the Kolmogorov scale would not be sufficient. However, the statistics shown here are not sensitive to this. There are other statistics that would require full resolution for accuracy, but these are not considered here. So to reduce the computational cost only 30 LEM cells per LEM line were used in the simulation.

The computational domain was decomposed into 120 processor domains using a simple algorithm having 8, 3 and 5 processor domains in x, y and z direction, respectively. One simulation time step in Kong et al. [2] took around 1 second while one LES-LEM simulation time step took 9 seconds, which can be explained by the fact that LES-LEM has to perform 2 splicing iterations (the most time consuming process), advance the solution on LEM lines (molecular diffusion and triplet maps) and copy the ghost LEM lines across the processor boundaries. For copying the ghost LEM lines, basic MPI (Message Passing Interface) functionalities were used and an efficient communication was achieved by sending/receiving data for one processor boundary at a time, i.e. communicating big chunks of data less often using bookkeeping.

3.2 Results and discussions

The results from the simulations were compared with the experiments at the middle z-normal plane at the same four downstream locations as done by Kong et al. [2], i.e. x/d = 1, 4.5, 7.5 and 12 (where d = 2cm).

Figure 3.2 and 3.3 show plots of the instantaneous velocity and the sub-grid turbulent kinetic energy field respectively at the middle z-normal plane.

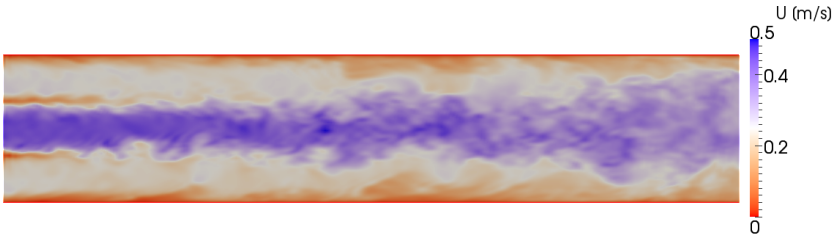

Figure 3.2: Instantaneous velocity contour plot in the middle z-normal plane at simulation time = 2.4 seconds

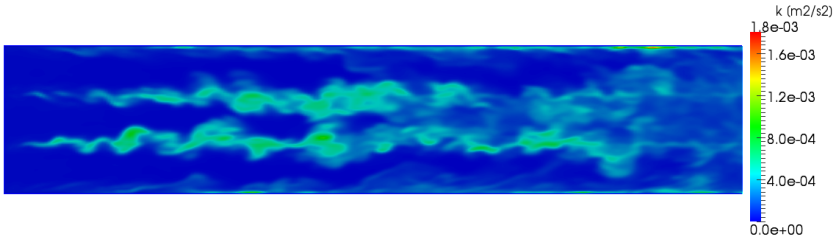

Figure 3.3: Instantaneous sub-grid turbulent kinetic energy contour plot in the middle z-normal plane at simulation time = 2.4 seconds

As the test case is a passive scalar mixing test case, the LES velocity field is not influenced by the LEM sub-grid model. This will be completely different for a combustion test case.

Figure 3.4 shows good agreement for the mean streamwise velocity profiles. Initially the flow is similar to a planar jet but further downstream the outer streams mix with the inner stream and a fully developed channel flow is achieved.

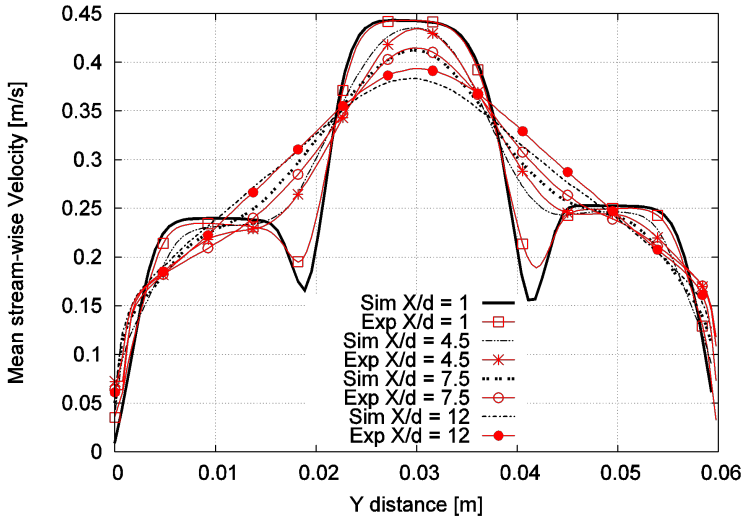

Figure 3.4: Mean streamwise velocity profiles at the four downstream locations

Figure 3.5 shows the streamwise rms velocity profiles. Close agreement can be seen between the simulations and the experiments. At x/d=1, two highly turbulent regions located at the tips of the splitter plates are formed due to merging of turbulent boundary layers from both sides of the splitter plates. It can be seen from Figure 3.5 that the streamwise rms velocity is high at the locations with high mean shear, i.e. wall boundary layers and mixing layers between the center jet and the outer streams. However, at the downstream locations, mean shear is reduced between the center jet and the outer streams resulting in reduced peaks.

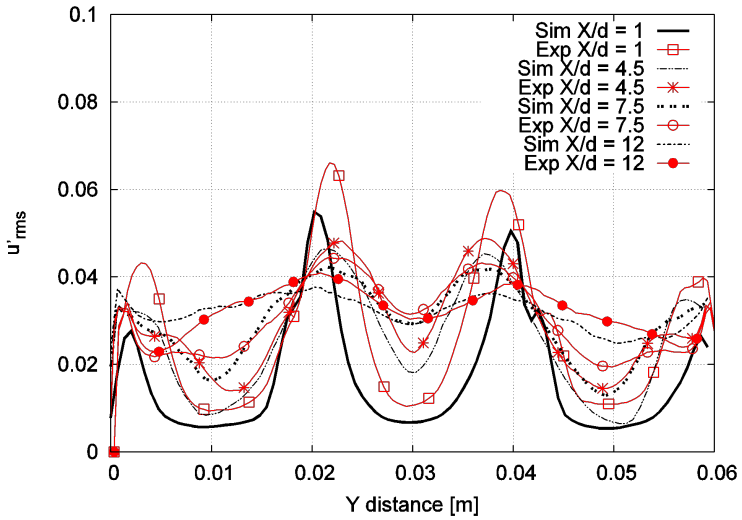

Figure 3.5: Streamwise rms velocity profiles at the four downstream locations

Figure 3.6 shows good agreement for the cross-stream rms velocity profiles and it can be seen that the profiles are similar to the stream-wise rms profiles in Figure 3.5 but peaks are a bit lower. In jet and shear layer flows, the cross-stream velocity is responsible for high mass and momentum transfer in those directions.

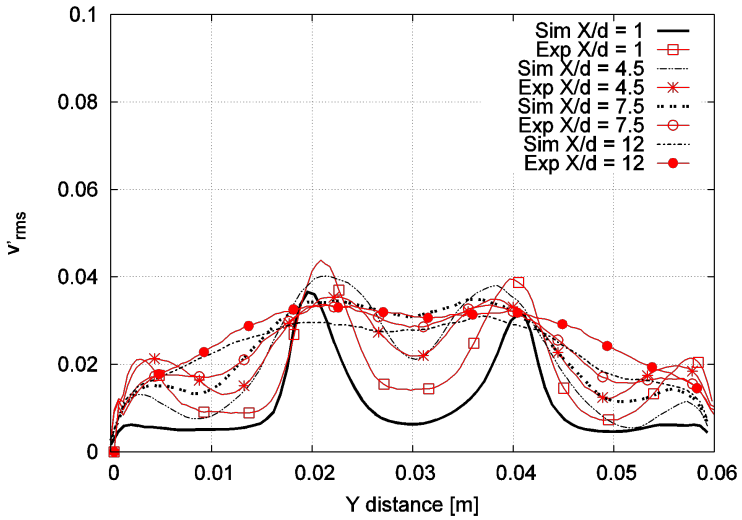

Figure 3.6: Cross-stream rms velocity profiles at the four downstream locations

The Reynolds shear stress is responsible for turbulent growth and spreading of a jet and its comparison is shown in Figure 3.7. As the profiles of mean velocity (which represent growth of a jet) in Figure 3.4 are matching, this suggests that the profiles of Reynolds stresses should also match which can be seen in Figure 3.7.

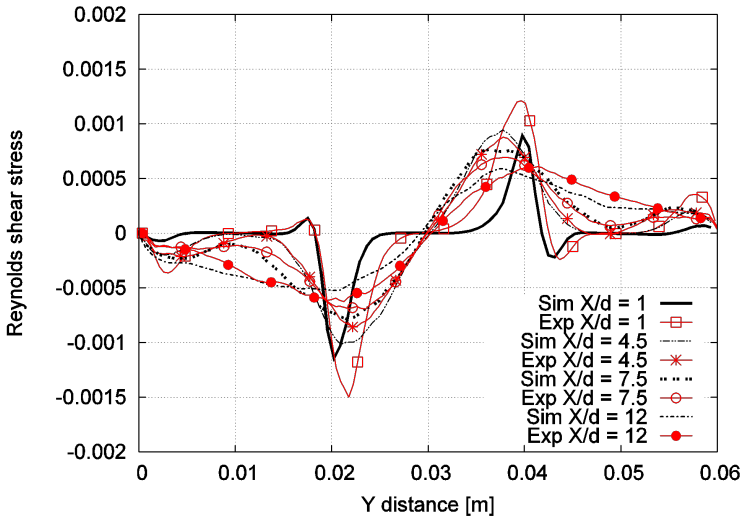

Figure 3.7: Reynolds shear stress profiles at the four downstream locations

Overall, the simulations are predicting the velocity statistics successfully, which is crucial for simulating passive scalar mixing.

3.2.1 Passive scalar mixing

At the inlet, the passive scalar was assigned a value of one in the middle stream and zero in the two side streams. Figure 3.8 shows plot of the instantaneous passive scalar field at the middle z-normal plane.

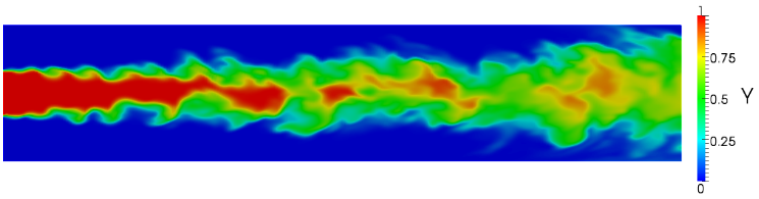

Figure 3.8: Instantaneous scalar contour plot in the middle z-normal plane at simulation time = 2.4 seconds

The mean scalar profiles are shown in Figure 3.9. Predictions from the simulations are close to the experimental results. Close to the inlet (at x/d=1) the mean passive scalar profile is bell shaped and becomes broad and flat with increasing distance from the inlet.

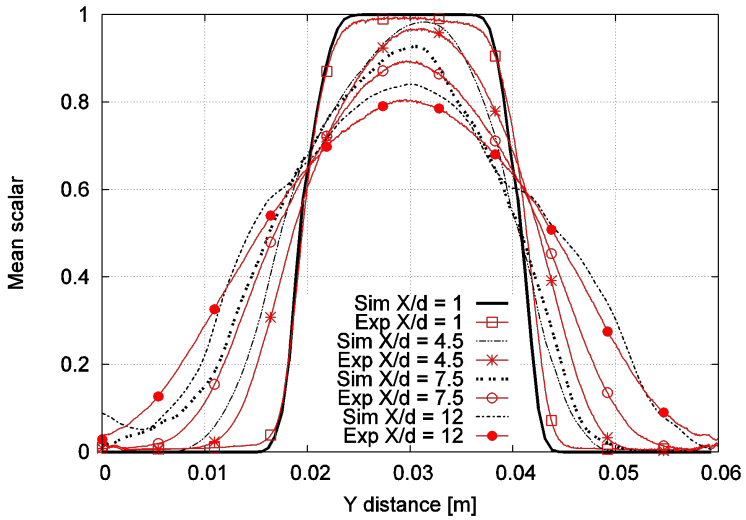

Figure 3.9: Mean scalar profiles at the four downstream locations

Figure 3.10 shows good agreement for the scalar fluctuations (i.e. rms values). It can be seen from Figure 3.10 that the scalar fluctuation peaks are observed in shear layers at the locations of the highest mean scalar gradient and mean velocity gradient. The locations of the scalar fluctuation peaks are away from the jet center than peaks observed in the streamwise and the cross-stream velocity fluctuations.

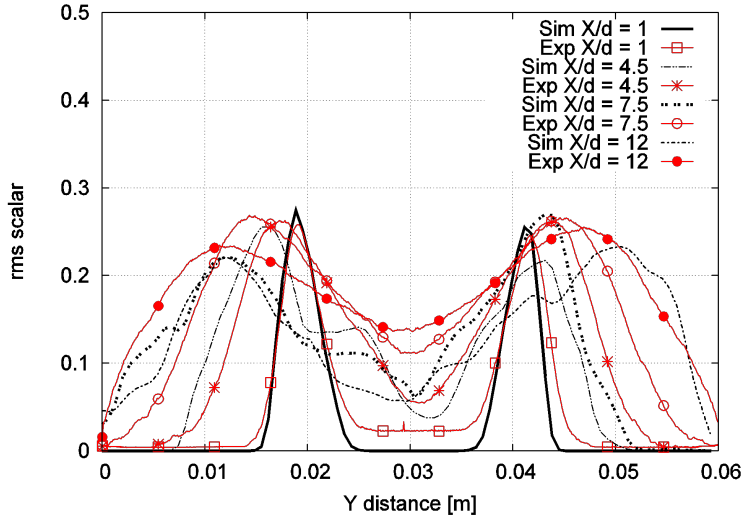

Figure 3.10: Scalar rms profiles at the four downstream locations

Chapter 4

LES-LEM for combustion

The overall goal for the current PhD project is combustion. Therefore, this chapter provides the LES equations for combustion (variable density and non-isothermal flow). The later part of this chapter describes coupling of the LES to the LEM sub-grid combustion model.

4.1 LES

The resulting LES equations for combustion simulations (after applying the spatial filter) for momentum, continuity, total energy and species conservation are:

$$\frac{\partial \overline{\rho}\widetilde{u}_i}{\partial t} + \frac{\partial}{\partial x_j}\left[\overline{\rho}\widetilde{u}_i\widetilde{u}_j + \overline{\rho}\delta_{ij} - \overline{\tau_{ij}} + {\tau_{ij}}^{sgs}\right] = 0, \tag{4.1}$$

$$\frac{\partial \overline{\rho}}{\partial t} + \frac{\partial \overline{\rho}\widetilde{u}_i}{\partial x_i} = 0, \tag{4.2}$$

$$\frac{\partial \overline{\rho}\widetilde{E}}{\partial t} + \frac{\partial}{\partial x_i}\left[\left(\overline{\rho}\widetilde{E} + \overline{p}\right)\widetilde{u}_i + \overline{q}_i - \widetilde{u}_j\overline{\tau_{ij}} + {H_i}^{sgs} + {\sigma_i}^{sgs}\right] = 0, \tag{4.3}$$

$$\frac{\partial \overline{\rho}\widetilde{Y_k}}{\partial t} + \frac{\partial}{\partial x_i}\left[\overline{\rho}\left(\widetilde{Y_k}\widetilde{u}_i + \widetilde{Y_k}\widetilde{V_{i,k}}\right) + {Y_{i,k}}^{sgs} + {\theta_{i,k}}^{sgs}\right] = \overline{\dot{\omega}_k} \qquad k = 1, ..., N_s, \tag{4.4}$$

where N_s is the total number of species. Here $(\overline{*})$ denotes spatial filtered values and $(\widetilde{*})$ denotes Favre averaged values defined for any variable as: $\widetilde{f} = \overline{\rho f}/\overline{\rho}$. In the above equations (4.1 - 4.4), E, Y_k, $\dot{\omega}_k$ and q denote total energy, species mass fraction, reaction rate and energy flux due to thermal conduction and species diffusion respectively. The total energy $\widetilde{E}$ is given by:

$$\widetilde{E} = \widetilde{e} + \frac{1}{2}\widetilde{u_k}\widetilde{u_k} + k^{sgs},$$

where $\widetilde{e}$ is the filtered internal energy and k^{sgs} is the sub-grid kinetic energy given by:

$$k^{sgs} = \frac{1}{2}[\widetilde{u_k u_k} - \widetilde{u_k}\widetilde{u_k}],$$

The filtered viscous shear stress $\overline{\tau_{ij}}$ in equation (4.1) is approximated as:

$$\overline{\tau_{ij}} = \overline{\mu}\left(\frac{\partial \widetilde{u_i}}{\partial x_j} + \frac{\partial \widetilde{u_j}}{\partial x_i}\right) - \frac{2}{3}\overline{\mu}(\frac{\partial \widetilde{u_k}}{\partial x_k})\delta_{ij},$$

where μ is the dynamic viscosity. The heat flux vector $\overline{q_i}$ from equation (4.3) is given by:

$$\overline{q_i} = -\overline{\kappa}\frac{\partial \widetilde{T}}{\partial x_i} + \overline{\rho}\sum_{k=1}^{N_s}\widetilde{h_k}\widetilde{Y_k}\widetilde{V_{i,k}} + \sum_{k=1}^{N_s} {q_{i,k}}^{sgs},$$

where $\overline{\kappa}$ and $\widetilde{h_k}$ denote the mean thermal mixture conductivity and the Favre averaged kth specie enthalpy respectively. The diffusion velocities $\widetilde{V_{i,k}}$ are approximated as:

$$\widetilde{V_{i,k}} = \big(-\frac{\widetilde{D_k}}{\widetilde{Y_k}}\big)\big(\frac{\partial \widetilde{Y_k}}{\partial x_i}\big),$$

where $\widetilde{D_k}$ is the Favre averaged kth specie diffusion coefficient. $\overline{p}$ from equation (4.3) is the filtered pressure calculated from the filtered equation of state:

$$\overline{p} = \overline{\rho}\widetilde{R}\widetilde{T} + \overline{\rho}T^{sgs},$$

Here, $\widetilde{R}$ is the mixture gas constant.

Filtering the conservation equations leads to (4.1 - 4.4) containing many unresolved sub-grid scale terms, denoted by superscript sgs, which need to be modelled. These sub-grid terms τ_{ij}^{sgs}, H_i^{sgs}, σ_i^{sgs}, $Y_{i,k}^{sgs}$, $\theta_{i,k}^{sgs}$ T_k^{sgs} and $q_{i,k}^{sgs}$ are the sub-grid shear stress, the sub-grid viscous work, the sub-grid viscous stress, the sub-grid mass flux, the sub-grid diffusive mass flux, the sub-grid temperature-species correlation and the sub-grid heat flux via turbulent convection of species, respectively. They are defined as:

$$
\begin{aligned}
{\tau_{ij}}^{sgs} &= \overline{\rho}\big(\widetilde{u_i u_j} - \widetilde{u}_i\widetilde{u}_j\big),\\
{H_i}^{sgs} &= \overline{\rho}\big(\widetilde{E u_i} - \widetilde{E}\widetilde{u}_i\big) + \big(\overline{\rho u_i} - \overline{\rho}\widetilde{u}_i\big),\\
{\sigma_i}^{sgs} &= \widetilde{u_j \tau_{ij}} - \widetilde{u}_j\overline{\tau_{ij}},\\
{Y_{i,k}}^{sgs} &= \overline{\rho}\big(\widetilde{u_i Y_k} - \widetilde{u}_i\widetilde{Y}_k\big),\\
{\theta_{i,k}}^{sgs} &= \overline{\rho}\big(\widetilde{V_{i,k} Y_k} - \widetilde{V_{i,k}}\widetilde{Y}_k\big),\\
{T_k}^{sgs} &= \big(\widetilde{Y_k T} - \widetilde{Y}_k\widetilde{T}\big),\\
{q_{i,k}}^{sgs} &= \left(\overline{h_k D_k \frac{\partial Y_k}{\partial x_i}} - \widetilde{h}_k\widetilde{D}_k\frac{\partial \widetilde{Y}_k}{\partial x_i}\right),
\end{aligned}
$$

The sub-grid small scales account for turbulent micro-mixing on the non-resolved scales. It is common practise and a well established approach to provide closure for the sub-grid shear stress ${\tau_{ij}}^{sgs}$ and the sub-grid viscous work (heat flux) ${H_i}^{sgs}$ with eddy-viscosity type models. There is no need to explicitly provide closures for the sub-grid mass flux ${Y_{i,k}}^{sgs}$, the sub-grid diffusive flux ${\theta_{i,k}}^{sgs}$ and the reaction rate $\overline{\dot{\omega_k}}$, as their closures are implemented in the sub-grid LEM combustion model. Other sub-grid terms are neglected here.

4.2 LEM

LEM solves the 1-D equations for species-mass and temperature as:

$$\frac{\partial \rho Y_k}{\partial t} + F_{k,stir} - \frac{\partial}{\partial x}\big(\rho D_k \frac{\partial Y_k}{\partial x}\big) = \dot{\omega_k} W_k, \tag{4.5}$$

$$\rho c_{p,mix}\frac{\partial T}{\partial t} + F_{T,stir} - \sum_{k=1}^{N_s}\rho c_{p,k} D_k(\frac{\partial Y_k}{\partial x})(\frac{\partial T}{\partial x}) - \frac{\partial}{\partial x}(\overline{\kappa}\frac{\partial T}{\partial x}) = -\sum_{k=1}^{N_s} h_k \dot{\omega_k} W_k, \tag{4.6}$$

where x and W_k denote the LEM domain co-ordinate direction and the molecular weight of kth specie respectively. $F_{k,stir}$ and $F_{T,stir}$ are of the form $\rho u(\frac{\partial Y_k}{\partial x})$ and $\rho u(\frac{\partial T}{\partial x})$ and they represent the turbulent convection of species and temperature respectively. $F_{k,stir}$ and $F_{T,stir}$ are modelled using triplet maps. $c_{p,k}$ and $c_{p,mix}$ denote the specific heat at constant pressure for kth specie and mixture respectively.

4.3 LES-LEM coupling

LES-LEM coupling is shown in Figure 4.1. As the LEM solves for temperature and specie-mass fractions in equations (4.5-4.6), there is no need to solve the corresponding LES equations, i.e. energy equation (4.3) and specie-mass fractions equation (4.4). The resolved LES field provides the local LES filter width and sub-grid turbulent kinetic energy to the LEM in order to calculate the local sub-grid Reynolds number. After performing the sub-grid calculations till the LES time step, the LEM provides filtered quantities, i.e. species-mass fractions and temperature to the resolved LES field. The filtered quantities are calculated as:

$$\widetilde{T_i} = \frac{\sum_{i=1}^{N_{LEM}} \rho_i T_i}{\sum_{i=1}^{N_{LEM}} \rho_i},$$

and

$$\widetilde{Y_{k_i}} = \frac{\sum_{i=1}^{N_{LEM}} \rho_i Y_{k_i}}{\sum_{i=1}^{N_{LEM}} \rho_i},$$

where N_{LEM} denotes total number of LEM cells in the LEM line.

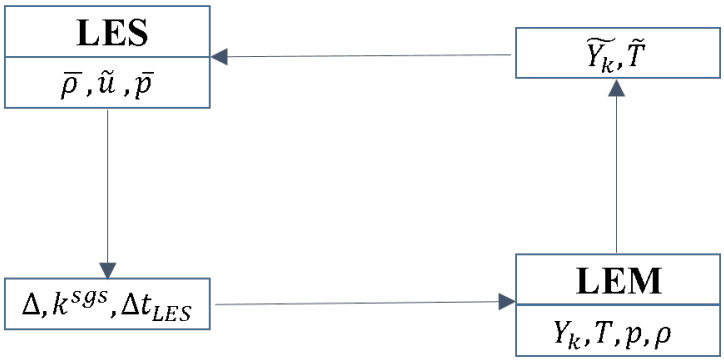

Figure 4.1: LES-LEM coupling

Chapter 5

Conclusion

In this licentiate thesis, the Linear Eddy Model (LEM) of Kerstein [1] was used as a sub-grid mixing model for Large Eddy Simulations (LES) called LES-LEM. In LES-LEM, LEM solves molecular diffusion and models sub-grid turbulent advection. Large scale scalar advection is modeled by a method called splicing. A new splicing strategy based on an ordered flux of spliced LEM segments was implemented in a pressure based fluid solver in OpenFOAM. The focus of the thesis was to qualitatively and quantitatively explore LES-LEM for passive scalar mixing. Therefore, LES-LEM combined with the new splicing approach was tested by simulating passive scalar mixing in a co-flowing turbulent liquid jet and the simulation results were compared to the experiments. It was shown that the simulations correctly predict velocity statistics and passive scalar mixing. Given that, LEM used as a sub-grid combustion model for LES, has been successfully applied to both premixed and non-premixed combustion and is regarded as a truly mode (premixed/non-premixed) and regime (fast/non fast chemistry) independent combustion model, the future work will be using LEM as a sub-grid combustion model for LES (for testing combustion cases).

References

[1] Kerstein, A. R., "Linear eddy modeling of turbulent transport and mixing," *Combustion Science and Technology*, 60:391-421, 1988.

[2] Kong, B., Olsen, M. G., Fox, R. O., Hill, J. C., "Predictive capability of Large Eddy Simulation for point-wise and spatial turbulence statistics in a confined rectangular jet," *Chemical Engineering Science*, 69:240-256, 2012.

[3] Pitsch, H., "Large-Eddy simulation of turbulent combustion," *Annual Review of Fluid Mechanics*, 38(4):453-482, 2006.

[4] Jhavar, R. and Rutland, C. J., "Using Large Eddy Simulations to Study Mixing Effects in Early Injection Diesel Engine Combustion," *SAE Technical Paper*, 2006-01-0871, 2006.

[5] Adomeit, P., Lang, O., Pischinger, S., Aymanns, R., Graf, M., Stapf, G., "Analysis of Cyclic Fluctuations of Charge Motion and Mixture Formation in a DISI Engine in Stratified Operation," *SAE Technical Paper*, 2007-01-1412, 2007.

[6] Yu, R., Bai, X. S., Hildingsson, L., Hultqvist, A., Miles, P. C., "Numerical and Experimental Investigation of Turbulent Flows in a Diesel Engine," *SAE Technical Paper*, 2006-01-3436, 2006.

[7] Yu, R. X., Bai, X. S., Vressner, A., Hultqvist, A., Johansson, B., Olofsson, J., Seyfried, H., Sjoholm, J., Richter, M., Alden, M., "Effect of Turbulence on HCCI Combustion," *SAE Technical Paper*, 2007-01-0183, 2007.

[8] Joelsson, T., Yu, R., Bai, X. S., Vressner, A., Johansson, B., "Large Eddy Simulation and Experiments of the Auto-Ignition Process of Lean Ethanol/Air Mixture in HCCI Engines ," *SAE International Journal of Fuels and Lubricants*, 1(1):1110-1119, 2008.

[9] Rutland, C. J., "Large-eddy simulations for internal combustion engines - a review," *International Journal of Engine Research*, 12(5):421-451, 2011.

[10] Kerstein, A. R., "Linear-eddy modeling of turbulent transport. Part 7. Finite-rate chemistry and multi-stream mixing," *Combustion Science and Technology*, 81:75-96, 1992.

[11] Kerstein, A. R., "Linear-eddy modeling of turbulent transport. II: Application to shear layer mixing" *Combustion and Flame*, 75:397-413, 1989.

[12] Kerstein, A. R., "Linear-eddy modeling of turbulent transport. III," *Journal of Fluid Mechanics*, 216:411-435, 1990.

[13] Kerstein, A. R., " Linear-eddy modeling of turbulent transport. Part 6. Microstructure of diffusive scalar mixing," *Journal of Fluid Mechanics*, 231:361-394, 1991.

[14] Kerstein, A. R., " Linear-eddy modeling of turbulent transport. Part V: Geometry of scalar interfaces," *Physics of Fluids A*, 3(5):1110-1114, 1991.

[15] McMurtry, P. A., Menon, S., Kerstein, A. R., "A linear eddy sub-grid model for turbulent reacting flows: Application to hydrogen-AIR combustion," *Proceedings of the Combustion Institute*, 24:271-278, 1992.

[16] Calhoon, W. H., "On subgrid combustion modeling for large-eddy simulations," *PhD thesis, Georgia Institute of Technology, Atlanta, GA*, 1996.

[17] Menon, S., Calhoon, W. H., "Subgrid mixing and molecular transport modeling in a reacting shear layer," *Proceedings of the Combustion Institute*, 26:59-66, 1996.

[18] Smith, T. M., "Unsteady simulations of turbulent premixed reacting flows," *PhD thesis, Georgia Institute of Technology, Atlanta, GA*, 1998.

[19] Chakravarthy, V. K., Menon, S., "Subgrid Modeling of Turbulent Premixed Flames in the Flamelet Regime," *Flow, Turbulence and Combustion*, 65:133-161, 2000.

[20] Pannala, S., Menon, S., "Large eddy simulations of two-phase turbulent flows," *36th AIAA Aerospace Sciences Meeting and Exhibit*, 98-0163, 1998.

[21] Zimberg, M. J., Frankel, S. H., Gore, J. P., Sivathanu, Y. R., "A Study of Coupled Turbulent Mixing, Soot Chemistry, and Radiation Effects Using the Linear Eddy Model" *Combustion and Flame*, 113:454-469, 1998.

[22] Sankaran, V., Menon, S., "Subgrid combustion modeling of 3-D premixed flames in the thin-reaction-zone regime," *Proceedings of the Combustion Institute*, 30:575-582, 2005.

[23] Sen B. A., Menon, S., "Linear eddy mixing based tabulation and artificial neural networks for large eddy simulations of turbulent flames" *Combustion and Flame*, 157:62-74, 2010.

[24] Sen B. A., Hawkes, E. R., Menon, S., "Large eddy simulation of extinction and reignition with artificial neural networks based chemical kinetics" *Combustion and Flame*, 157:566-578, 2010.

[25] Ochoa, J. S., Sanchez-Insa. A., Fueyo, N., "Subgrid Linear Eddy Mixing and Combustion Modelling of a Turbulent Nonpremixed Piloted Jet Flame," *Flow, Turbulence and Combustion*, 89:295-309, 2012.

[26] Sone K., Menon, S., "Effect of Subgrid Modeling on the In-Cylinder Unsteady Mixing Process in a Direct Injection Engine" *Journal of Engineering for Gas Turbines and Power*, 125(2):435-443, 2003.

[27] Steeper, R., Sankaran, V., Oefelein, J., Hessel, R., "Simulation of the Effect of Spatial Fuel Distribution Using a Linear-Eddy Model," *SAE Technical Paper*, 2007-01-4131, 2007.

[28] Maxwell B. M., Falle, S. A. E. G., Sharpe, G., Radulescu, M. I., "A compressible-LEM turbulent combustion subgrid model for assessing gaseous explosion hazards" *Journal of Loss Prevention in the Process Industries*, 36:460-470, 2015.

[29] Martinez, D. M., Jiang, X., Moulinec, C., Emerson, D. R., "Numerical simulations of turbulent jet flames with non-premixed combustion of hydrogen-enriched fuels" *Computers and Fluids*, 88:688-701, 2013.

[30] Martinez, D. M., Jiang, X., Moulinec, C., Emerson, D. R., "Numerical assessment of subgrid scale models for scalar transport in large-eddy simulations of hydrogen-enriched fuels" *International Journal of Hydrogen Energy*, 39:7173-7189, 2014.

[31] Lovett, J. A., Ahmed, K., Bibik, O., Smith, A. G., Lubarsky, E., Menon, S., Zinn, B. T., "On the Influence of Fuel Distribution on

the Flame Structure of Bluff-Body Stabilized Flames" *Journal of Engineering for Gas Turbines and Power*, 136(4), 041503, 2013.

[32] Srinivasan, S., Kozaka, E. O., Menon, S., "A New Subgrid Breakup Model for LES of Spray Mixing and Combustion" *Direct and Large-Eddy Simulation VIII, ERCOFTAC, Springer science and Business Media*, 333-338, 2011.

[33] Srinivasan, S., Ranjan, R., Menon, S., "Flame Dynamics During Combustion Instability in a High-Pressure, Shear-Coaxial Injector Combustor," *Flow, Turbulence and Combustion*, 94:237-262, 2015.

[34] Vedula, P., Yeung, P. K., Fox, R. O., "Dynamics of scalar dissipation in isotropic turbulence: a numerical and modelling study," *Journal of Fluid Mechanics*, 433:29-60, 2001.

[35] Donzis, D. A., Yeung, P. K., "Resolution effects and scaling in numerical simulations of passive scalar mixing in turbulence," *Physica D*, 239:1278-1287, 2010.

[36] Cha, C. M., Kops, S. M. B., Mortensen, M., "Direct numerical simulations of the double scalar mixing layer. Part I: Passive scalar mixing and dissipation," *Physics of Fluids*, 18, 067106, 2006.

[37] Sawford, B. L., Kops, S. M. B., "Direct numerical simulation and Lagrangian modeling of joint scalar statistics in ternary mixing," *Physics of Fluids*, 20, 095106, 2008.

[38] Akselvoll, K., Moin, P., "Large-eddy simulation of turbulent confined coannular jets," *Journal of Fluid Mechanics*, 315:387-411, 1996.

[39] Kang, H. S., Meneveau, C., "Passive scalar anisotropy in a heated turbulent wake: new observations and implications for large-eddy simulations," *Journal of Fluid Mechanics*, 442:161-170, 2001.

[40] Dong, Y. H., Lu, X. Y., Zhuang, L. X., "An investigation of the Prandtl number effect on turbulent heat transfer in channel flows by large eddy simulation," *Acta Mechanica*, 159:39-51, 2002.

[41] Philips, D. A., Rossi, R., Iaccarino, G., "Large-eddy simulation of passive scalar dispersion in an urban-like canopy," *Journal of Fluid Mechanics*, 723:404-428, 2013.

[42] Mejia, J. M., Sadiki, A., Molina, A., Chejne, F., Pantangi, P., "Large Eddy Simulation of the Mixing of a Passive Scalar in a High-Schmidt Turbulent Jet," *Journal of Fluids Engineering*, 137, 031301, 2015.

[43] Smagorinsky., J., "General circulation experiments with the primitive equations, I. The basic experiment," *Monthly Weather Review*, 91(3):99-164, 1963.

[44] Yoshizawa, A., "Statistical theory for compressible shear flows, with the application to subgrid modelling," *Physics of Fluids*, 29(7):2152-2164, 1986.

[45] Germano, M., Piomelli, U., Moin, P., Cabot., W. H., "A dynamic subgrid-scale eddy viscosity model," *Physics of Fluids A*, 3(7):1760-1765, 1991.

[46] Lilly, D. K., "A proposed modification of the Germano subgrid-scale closure method," *Physics of Fluids A*, 4(3):633-635, 1992.

[47] Sankaran, V., "Sub-grid combustion modeling for compressible two-phase reacting flows," *PhD thesis, Georgia Institute of Technology, Atlanta, GA*, 2003.

[48] Feng, H., Olsen, M. G., Liu, Y., Fox, R. O., Hill, J. C., "Investigation of turbulent mixing in a confined planar-jet reactor," *Journal of American Institute of Chemical Engineers*, 51:2649-2664, 2005.